

LINING TECHNOLOGY OF SATURATED SAND LAYER UNDERGROUND DIVERSION TUNNEL AND THE MEASUREMENT OF CONCRETE LINING THICKNESS

Tecnología de revestimiento de capa de arena saturada en túnel de desviación subterráneo y la medición del espesor de revestimiento del hormigón

Qixin LIU

School of Logistics, Chengdu University of Information Technology, Chengdu 610000, China.

E-mail: cdxxjs25@163.com

(Received: October 2021; accepted: March 2022)

Key words: Saturated sand formations, diversion tunnels, lining technology, non-destructive.

ABSTRACT

In order to improve the construction technology quality of the diversion tunnel lining in saturated sand stratum, the lining technology of underground diversion tunnel in saturated sand stratum is studied in detail in this paper. Steel trolley is used to complete binding production, and HBT-20 concrete pump is used to transport concrete. Concrete construction starts from bottom plate and side arch. After the construction, the quality of the diversion tunnel lining is tested nondestructively by the impact elastic wave, and the thickness and defects of the lining are analyzed by the reflection characteristics and spectral relationship of the impact elastic wave. The strength of lining concrete is measured by the propagation characteristics of R wave and the relationship between wave velocity and strength. The results show that the maximum additional bending strain of tunnel wall is about 300 $\mu\epsilon$. At measuring point B7, the thickness and strength of concrete lining can be accurately measured by nondestructive quality testing technology.

Palabras clave: formaciones de arena saturada, túneles de desviación, tecnología de revestimiento, no destructiva.

RESUMEN

Con el fin de mejorar la calidad de la tecnología de construcción del revestimiento del túnel de desviación en estrato de arena saturada, la tecnología de revestimiento del túnel de desviación subterránea en estrato de arena saturada se estudia en detalle en este documento. El carro de acero se utiliza para completar la producción de unión, y la bomba de hormigón HBT-20 se utiliza para transportar el hormigón. La construcción con hormigón comienza desde la placa inferior y el arco lateral. Después de la construcción, la calidad del revestimiento del túnel de desviación se prueba no destructivamente por la onda elástica de impacto, y el espesor y los defectos del revestimiento se analizan por las características de reflexión y la relación espectral de la onda elástica de impacto. La fuerza del revestimiento del hormigón se mide por las características de propagación de la onda R y la relación entre la velocidad de la onda y la fuerza. Los resultados muestran que la deformación adicional máxima de la pared del túnel es de aproximadamente 300 $\mu\epsilon$. En el punto de medición B7, el espesor y la resistencia del revestimiento del hormigón se pueden medir con precisión mediante tecnología de prueba de calidad no destructiva.

INTRODUCTION

With the development and utilization of underground space, there are more and more large-section and shallow underground structures. Previous earthquake damage has shown that these structures are vulnerable to earthquake damage. Liquefaction of saturated sand layers during earthquakes is one of the important reasons for the failure of underground structures (Lu et al. 2017). Under the action of earthquake, the pore water pressure of saturated sand foundation increases, the effective stress decreases to 0, the shear resistance is lost, and the soil exhibits fluid behavior (Galkaduwa et al. 2017, Zou et al. 2018). Tunnel linings are permanent structures that support and maintain the long-term stability of the tunnel. Its role is to support and maintain the stability of the tunnel, prevent the weathering of the surrounding rock, and mitigate the impact of groundwater (Ahmed et al. 2017). If the lining construction quality of the water diversion tunnel is not high during the construction of the stratum, it will cause the tunnel to collapse, which will have a great impact on the normal operation of the hydropower project. Therefore, the tunnel lining must have sufficient strength, durability, certain frost resistance, impermeability and erosion resistance. Based on this, it is very important to study the lining technology of underground diversion tunnel in saturated sand layer in this paper.

The tunnel lining is mainly composed of arch ring, side wall, inverted arch and bottom plate. After the tunnel is excavated, the balance of the stratum around the tunnel is destroyed, causing the tunnel to deform or collapse. In order to protect the stability of the surrounding rock, the underground diversion tunnel must have sufficient supporting structure, that is, the tunnel lining. Different surrounding rocks can adopt different lining forms (Xue et al. 2019). Commonly used lining forms are shotcrete lining, shotcrete bolt lining and composite lining. In most cases, a composite lining is used. Composite lining is usually divided into primary lining and secondary lining. Common materials are concrete and reinforced concrete, slate concrete, precast aggregate blocks or suspect soil, shotcrete, etc. (Chen et al. 2021, Walker et al. 2018). The tunnel lining structure form proposed by Zhao and Li (2020) is mainly determined based on the geological and topographic conditions of the tunnel, and the rationality of factors such as its structural stress, construction method and construction technology level. The structure, shape and size of tunnel linings vary by application, topography, geology, construction and structural performance.

Based on the above analysis, the lining quality of the underground diversion tunnel in saturated sand stratum is the key factor to ensure the stability of the tunnel. During the construction of a diversion tunnel, the quality of the concrete lining directly affects the long-term stability, normal operation and appearance of the tunnel (Huo et al. 2018). In order to ensure the quality of tunnel engineering, engineering quality inspection is an essential and important link. Therefore, this paper systematically studies the lining technology of saturated sandy aquifers.

The groundwater diversion tunnel lining technology studied in this paper adds a quality inspection link to the tunnel construction. Common quality problems of tunnel concrete lining are: concrete cracking and internal defects, insufficient concrete strength, insufficient lining thickness, steel corrosion and voids. The saturated sand underground diversion tunnel has the characteristics of circular section, single working face and harsh environment, which limit the application of many conventional methods to the quality inspection of concrete lining. In this study, the shock elastic wave method is proposed to solve the quality inspection problem of belted lining, including the strength and thickness inspection of lining concrete, and applied to specific projects (Lan et al. 2022). It can be said that the method in this paper provides effective support for improving the safety performance of underground tunnels in saturated sand layers and enhancing the seismic performance of tunnels.

MATERIALS AND METHODS

Lining construction technology of underground diversion tunnel

Steel bar production and concrete selection

(1) Production and binding of steel bars

The steel bar binding is made by the steel bar trolley binding. The overlap length of 3/4 and 1/4 joints occurs when binding steel bars. If the overlap length of 3/4 and 1/4 joints is staggered according to the design requirements (10 days from the joints), the excavation and lining cannot be carried out smoothly after concreting in a warehouse (Zuo et al. 2020). Therefore, the following tests are carried out:

The symmetrical position of 135° is selected, i.e. overlap of steel bars in places with less stress (Li et al. 2019); T502 welding rod is used to ensure the quality of weld; and after conservative calculation of the fourth strength theory, the minimum safety factor is 24 (Yang et al. 2020). In order to ensure that the quality and progress of the project can meet the

pressure water. After the foundation is cleaned, the construction parties shall jointly check and accept it and make geological sketches. Random bolts are arranged in the places where geological defects exist, and loosened rocks are cleared.

(3) Layout of erecting bars and measurement setting-out

Hand-air drilling is used to drill holes in the inner side of the slit line of the construction block. The depth of the hole is 30 m-50 cm and the diameter of the hole is 42 mm. The steel bars with $\Phi 25$ m are inserted into the hole to make the vertical reinforcement. The row distance between the vertical reinforcement is 1.5 m. Horizontal reinforcing bars are welded between the vertical reinforcement and the side wall anchor rods to mark and measure the alignment points. According to the setting-off point given by the measurement, the bottom elevation of the structural steel bar is manually released by horizontal pipe, and the horizontal erection bar is welded to support the structural steel bar.

(4) Reinforcement installation

Rebar shall be laid according to construction drawings, design notices or other design requirements. The installation of reinforcing bars adopts binding method, the overlap of stress bars uses one-sided welding, and the welding length is not less than 20 D. The thickness of the protective layer should be specially controlled, and the large surface of the reinforcing bar net should be smooth. Other installation requirements of reinforcing bars shall be carried out according to the design requirements.

(5) Installation of water stop and plug formwork

Rubber water stop is installed at the joint of concrete structure in diversion tunnel. Its thickness is 8 mm and width is 28 cm. The joint is lapped and the lap length is not less than 20 cm. The plug formwork is assembled with combined steel die, partially with wood die to mend the joint, and the formwork is fixed with tension bar (Ziaei and Ahangari 2018). When the plug formwork is installed to the water stop height, the rubber water stop belt is laid on the formwork, and the water stop belt is fixed with steel hook of $\Phi 16$ mm and steel bracket of $\Phi 22$ mm, and then the upper formwork is supported. When the water stop is installed, the reinforcing steel bars cannot pass through the structural joints. At least 50 cm above the concrete pouring surface is protruded from the upper part of the water stop to meet the needs of the water stop joint.

(6) Preparing and checking warehouses before pouring

The preparation of bottom mud condensate pouring mainly includes scraper rail installation, construction platform erection, warehouse cleaning, vibration ramming equipment and concrete pump truck positioning, etc.

(7) Concrete pouring

The concrete is used to pump 2 m³-3 m³ mortar in the first place when the coagulant is poured. The silo is covered with the thickness of 2 cm-3 cm, and the mortar and the clay are with the same label. The slump of concrete is controlled between 14 cm and 18 cm. The slump of concrete is monitored by laboratory personnel and adjusted at any time (Wang et al. 2017). If the stopping time is too long but the initial setting time is not yet reached, the concrete can be poured with the same label mortar after obtaining the supervision's consent. The thickness of concrete pouring layer should be controlled within 30 cm-40 cm.

Next, we will carry out the work of smearing and maintenance.

Concrete construction of side arch

(1) Joint surface treatment, survey setting-out and drainage tank construction

Before the final setting of floor concrete, high-pressure water is used to flush the concrete section of side wall, and artificial chisel is used in part. When flushing, it should pay attention to protecting the floor concrete surface. The design elevation and side line are measured on the spot, the measuring points are marked on the erecting steel bar, and the erecting steel bar is welded and fixed on the structural steel bar and the side wall anchor.

Construction of drainage tank. On the concrete joints of the bottom slabs of the two sides of the walls, a square groove with 10 cm \times 35 cm (width \times depth) is drilled along the rock wall side. After washing and drying, the groove is filled with clean pebbles, covered with geotextiles, and reinforced with steel bars of $\Phi 12$ mm. By extending the PVC pipe of the side wall concrete, the water seepage from the rock wall is discharged out of the warehouse by the drainage trough.

(2) Positioning of steel mould trolley

The first assembly of the steel formwork trolley should be carried out after 2-4 pieces of concrete are poured into the bottom slab, and the track is laid on the mud-soil surface of the bottom slab after construction. The assembly of the steel formwork trolley uses

the space of the return lane, and lifts the separated steel formwork trolley into place with the anchor rod preset in the top arch and the hand-pulled hoist. The positioning of steel formwork trolley mainly depends on hoist and rail clamping device, and its operation should be carried out in strict accordance with the Instructions for the Use of Steel Formwork Trolley.

According to the selected steel bars for installation, a good job of pouring is prepared and warehouse is inspected, to start concrete pouring.

Nondestructive testing of lining quality of diversion tunnel based on shock elastic wave

Concrete lining quality detection is realized by using shock elastic wave theory and wave characteristics. The thickness and defects of concrete lining are analyzed by the reflection characteristics and frequency spectrum relationship of shock elastic wave, and the strength of concrete lining is tested by using the propagation characteristics of R wave and the correlation between wave velocity and strength.

Lining thickness detection

If the thickness of lining fails to meet the design requirements, it will affect the overall strength and durability of tunnel structure, resulting in hidden dangers and even serious engineering accidents. So, it is of great significance and practical value to test its thickness based on non-destructive testing method. This study is based on the transient low stress wave generated by shock vibration, which propagates into the structure and is reflected back by the bottom surface of the difference in defect and wave impedance. By analyzing the spectrum of the reflected signal, the thickness and defects of the lining can be deduced.

According to the thickness of lining, there are two main methods: one is to use echo repetitive reflection method (Fig. 1), which requires a certain number of reflections (usually more than eight effective reflections) and combines with a variety of spectrum analysis techniques (FFT, MEM, etc.) to test the thickness of lining. As shown in formula (1), this method is suitable for thinner lining; the other is signal direct identification method (Fig. 2). Thickness and defect can be analyzed directly by the time difference between the first wave and the bottom or the defect reflection. This method is suitable for the case of thick lining.

The formula for testing lining thickness is as follows:

$$\delta = \frac{V_p}{2f_c} \quad (1)$$

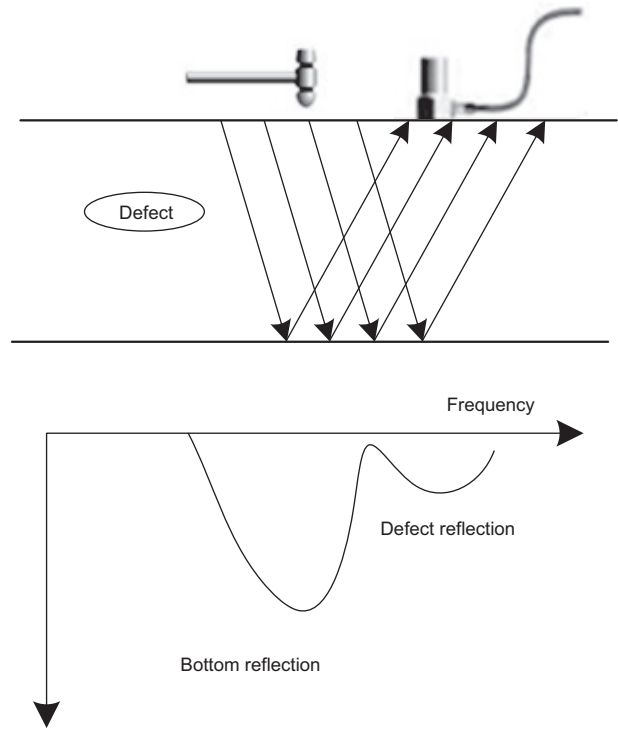


Fig. 1. Repeated reflection method for testing lining thickness and defects.

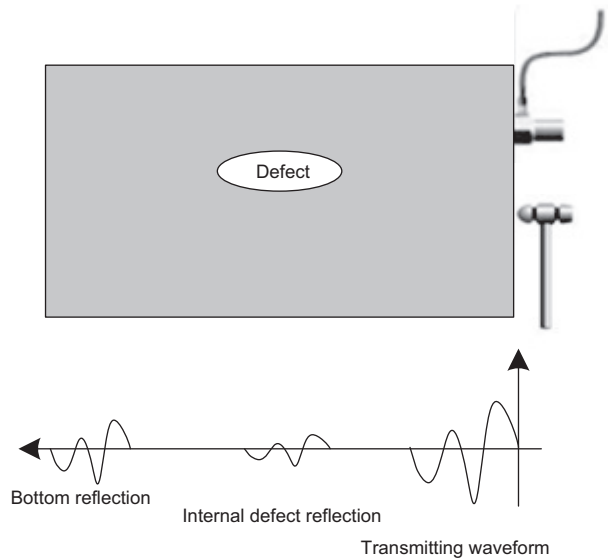


Fig. 2. Signal direct recognition method for testing lining thickness and defects.

In the formula, δ denotes the thickness of concrete lining, V_p denotes the P-wave velocity of elastic wave, and f_c denotes the resonance frequency of longitudinal wave.

Strength testing of concrete lining

Concrete strength testing technology is very mature. Generally speaking, it is based on various testing parameters (wave velocity, rebound value, pull-out force, etc.) to establish the relationship curve with concrete compressive strength. When there is only one test operation in the tunnel and the section is circular, the application of many test methods is limited (Klaver et al. 2017, Walsh et al. 2019). In this study, the velocity of R wave is used to measure concrete strength (Fig. 3). In essence, the velocity of R wave is obtained by dividing the distance between sensors by the time difference of R wave propagating in concrete. The relationship between R wave and P wave is converted to P wave velocity, and then concrete strength is obtained by P wave velocity and concrete strength formula (2). In concrete structures, Poisson's ratio is generally 0.15-0.1, while P-wave velocity is 1.73-1.79 times of R-wave velocity. In addition, in small concrete members, shock elastic wave velocity is 28% faster than P wave velocity measured by ultrasonic wave, while in large concrete structures there is almost no difference (Aboukila and Norton 2017), so the formula can be used to complete the calculation. Figure 4 is the accuracy verification of the test method in the laboratory. The static elastic

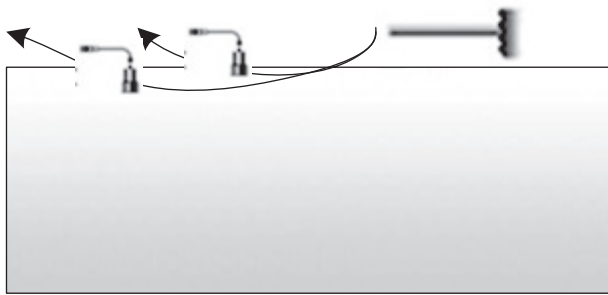


Fig. 3. R-wave measurement of concrete lining strength.

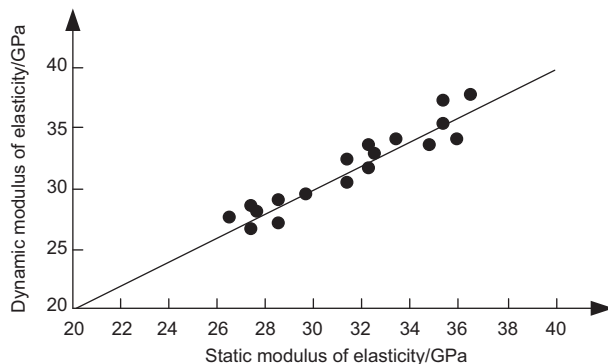


Fig. 4. Accuracy comparison of R wave test for concrete strength.

modulus and the dynamic elastic modulus are calculated and compared respectively. The dynamic elastic modulus is calculated based on formula (2). It can be seen that this method is feasible.

Formula (2) refers to the relationship between ultrasonic wave and compressive strength of ordinary concrete proposed by Japanese Architectural Society.

$$\sigma_c = 215V_{PU} - 620 \quad (2)$$

$$V_p = \sqrt{\frac{\delta}{f_c} \frac{1 - \sigma_c}{(1 + \sigma_c)(1 - 2\sigma_c)}} \quad (3)$$

In the formulas, V_{PU} and σ_c represent the ultrasonic and compressive strength of concrete respectively; Formula (3) is the ratio of static modulus of elasticity to dynamic modulus of elasticity.

Detection technology for lining concrete of diversion tunnel based on geological radar

According to the lining and grouting conditions of diversion tunnel, two aspects are tested:

(1) Determination the compactness of lining concrete. According to the radar image characteristics of concrete reflection radar electromagnetic wave, concrete bonding quality can be divided into two kinds: compact and non-compact. Concrete compactness refers to uniform vibration, uniform material and good pouring quality of concrete. In radar images, it shows clear image, uniform distribution of reflected energy of electromagnetic wave, slow energy attenuation (Zhu et al. 2017), good continuity of in-phase axis, stable waveform and strong regularity; non-compactness of concrete refers to poor compactness of concrete, non-uniform vibration, hollow local aggregate skeleton, and honeycomb separation. In radar images, the energy distribution of electromagnetic wave is not uniform, the energy attenuation is fast, and the local discrete phenomenon appears (Peng et al. 2017). The coaxial continuity is poor, and the waveform amplitude is unstable and disorderly.

(2) Judgment of the contact between concrete and surrounding rock. According to the radar image characteristics of the contact between concrete and surrounding rock, the contact between concrete and surrounding rock can be divided into three types: tight cementation, slight void and void. When the consolidation is tight, the radar image shows the electromagnetic wave reflected energy distribution is uniform and regular, the signal amplitude is small, the waveform is stable, the image is clear; slight void shows that the reflection waveform of the lining

cementation interface is cluttered, the energy intensity is irregular, and the phase is discontinuous, so the continuous coaxial cannot be traced in the profile, and there is obvious reflection phenomenon locally (Hu et al. 2018). The void is characterized by strong energy, abundant frequency component and wide frequency band of reflected radar wave from the lining cemented interface, forming a near-arc, continuous traceable reflection wave group on the profile, accompanied by multiple strong reflections (Gao and Wang 2017, Brown et al. 2018, Fernández-Pousa, 2018, Wu et al. 2018).

RESULTS

Project survey

Taking a diversion power station with daily regulation performance in the Yangtze River Basin as the research object, the design head of the power station is 312 m, the design flow is $30.6 \text{ m}^3/\text{s}$, the installed capacity is 80 MW, and the annual power generation is about 323 million kw/h (Tian et al. 2020). The main structures of the project hub include water intake hub, self-regulating pressure-free diversion tunnel, pressure forebay and penstock, power plant main and auxiliary plant, installation room, outdoor main transformer switch site and auxiliary plant ejection line site, etc. (Khellat and Khormizi 2018).

The actual scene of the water diversion tunnel of the power generation project is shown in **figure 5**.

In the saturated sand layer in the experimental area to be studied, the main composition is medium fine sand, and its relative density is about 40%. The



Fig. 5. Real view of the diversion tunnel.

sand grading and accumulation curve is shown in **figure 6**, and **table II** describes the main properties of medium and fine sand in the soil layer (Manitaras and Papadrakakis 2017).

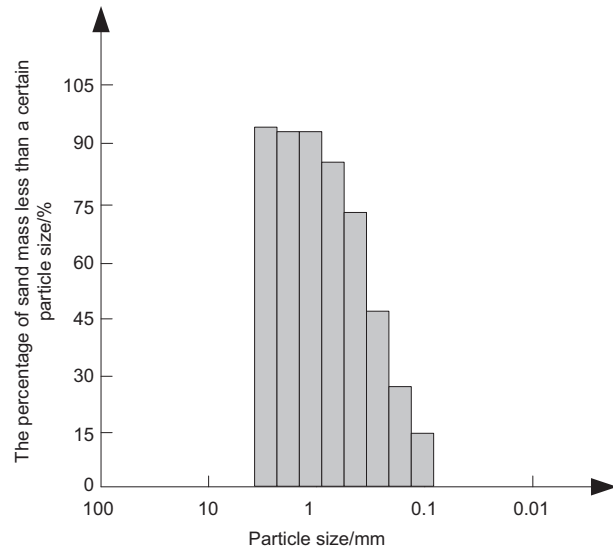


Fig. 6. Accumulative curve of sand gradation.

TABLE II. PROPERTIES PARAMETERS OF SAND IN EXPERIMENTAL AREA.

Property parameters of sandy soil	Numerical value
Mean diameter /mm	0.302
Coefficient of inhomogeneity	2.73
Specific gravity of soil particle	2.56
Permeability coefficient / $\text{cm} \cdot \text{s}^{-2}$	2.2
Maximum dry density / $\text{g} \cdot \text{cm}^{-3}$	1.626
Minimum dry density / $\text{g} \cdot \text{cm}^{-3}$	1.35
Maximum void ratio	0.817
Minimum void ratio	0.526

The diversion tunnel of the power station is a pressure-free tunnel with automatic regulation, and the design flow rate is $3.06 \text{ m}^3/\text{s}$. The total length of the tunnel is 5621.36 m. The elevation of the inlet floor is 1527.00 m, and the elevation of the floor is 1524.18 m at the gradient section of the forebay. The design section of the diversion tunnel is a city gate tunnel with a right angle at the bottom. Concrete lining and hanging net shotcrete are adopted. The cross section of the concrete lining is $4.2 \text{ m} \times 5.91 \text{ m} \sim 8.73 \text{ m}$. Among them, at pile number 3 + 0.31 m ~ 5 + 350 m, the width is changed to 5.2 m. Concrete lining is

adopted, the length of concrete section is 12 m, and the thickness of lining is 55 cm. The standard section of the tunnel is shown in **figure 7**.

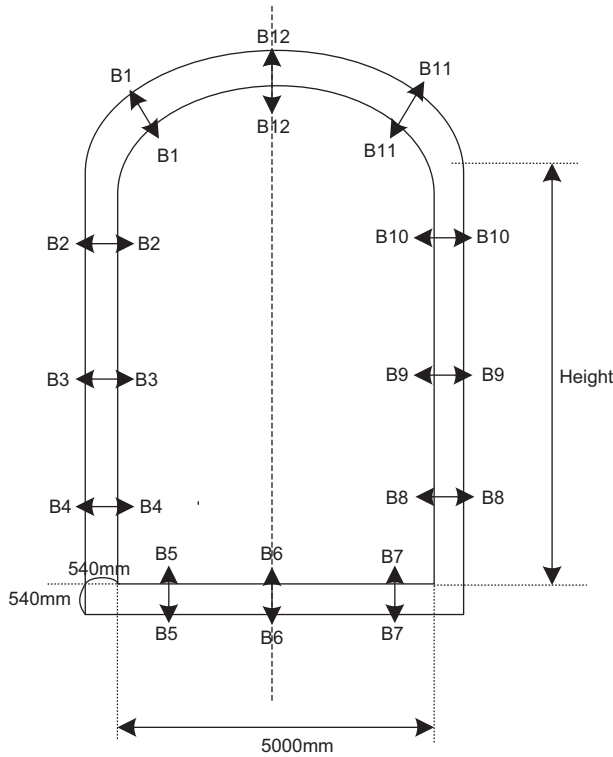


Fig. 7. Tunnel standard section and strain gauge monitoring layout/mm.

Tunnel strain change

In order to test the reliability of the lining project of the underground diversion tunnel constructed with the lining technology in this paper, the strain distribution of the tunnel is first examined. In order to ensure the validity and accuracy of the test, a certain period of 1600 seconds of the engineering time was selected for this test, during which bending strain is being caused by vibration caused by the earthquake. A total of 12 strain gauges were installed in this experiment, but because the display results of other strain gauges are similar, the purpose of this experiment cannot be highlighted, so only the data displayed by 4 strain gauges are analyzed, and the results are shown in **figure 8**. This figure shows the additional bending strain at some measuring points of tunnel wall caused by vibration (excluding the deformation under static load, the external wall is tensioned normally, and the arrangement of strain gauges is shown in **Fig. 7**).

It can be seen from the results of each measuring point that the additional strain can be regarded as the superposition of two parts: one is the additional strain caused by the gentle increase of soil and water pressure, which refers to the additional strain caused by the sand compactness and the gradual increase of total earth pressure caused by the increase of pore pressure during the vibration process; the other is the additional vibration strain caused by the earthquake process (Lakshminarayana et al. 2018). Earthquake acceleration makes the structure subject to inertia force. At the same time, soil vibration is reflected in the structure through the change of dynamic earth pressure, which results in additional strain of the structure, of which the former is the main part. Due to the influence of the change of soil-water pressure caused by vibration, the left and right sides of the structure are basically the same. With the dissipation of excess pore pressure in the later stage, the additional strain gradually decreases to 0.

The additional vibration strain is different in the course of earthquake. **Figure 9** intercepts the additional strain of the structure at the middle points of the left and right sides of the tunnel during vibration. It can be clearly seen that this part of the strain is inverse on the left and right sides of the structure. The maximum additional bending strain of tunnel wall caused by vibration is about $300 \mu\epsilon$, which appears at measuring point B7. The bending moment of the prototype section is 58.9 kN m/m , which is about 1/2 of the bending moment of the section under static load. If there is no flow between the bending strain and the strength of the concrete lining, the result of the bending strain is the regular monitoring of the new building structure. By monitoring and analyzing each test point, the strain result of the concrete strength is about $160 \mu\epsilon$.

Testing of thickness and strength of concrete lining

According to the strain gauge arrangement obtained from the above-mentioned tunnel strain change analysis, test points are installed at B1, B4, B6, B8, and B11 on the tunnel section, and shock elastic wave nondestructive testing is performed on 6 tunnel sections. The impact-echo detection method is used to test 30 concrete lining thickness values and 30 concrete strength values, and the low-frequency stress wave reflections generated by short-term mechanical shocks are used to be accepted by the sensor for amplitude spectrum analysis. **Table III** and **figure 10** show the lining thickness and concrete strength of a section, and five groups of data are measured on each section.

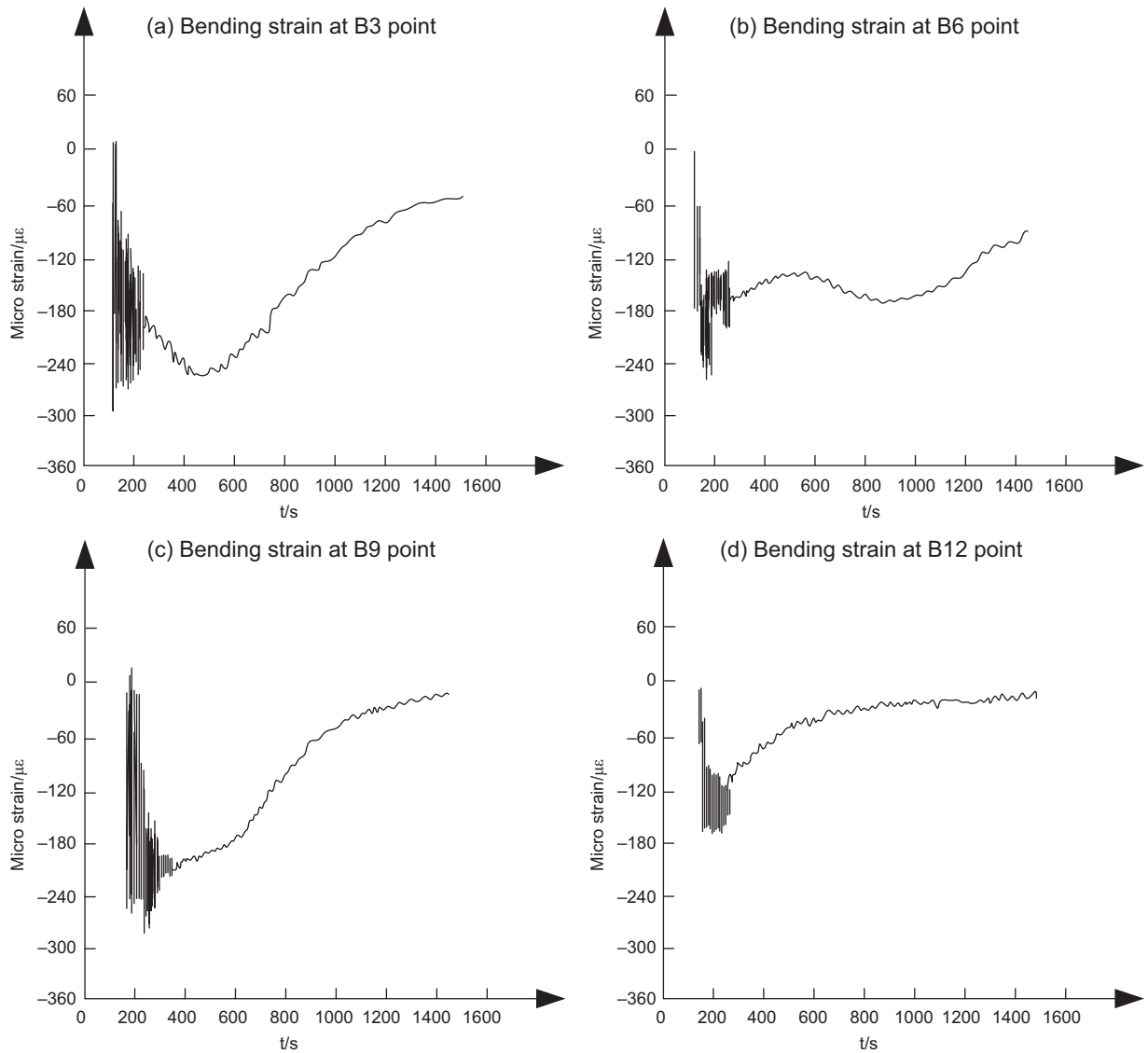


Fig. 8. Bending strain detection at some measuring points of diversion tunnel.

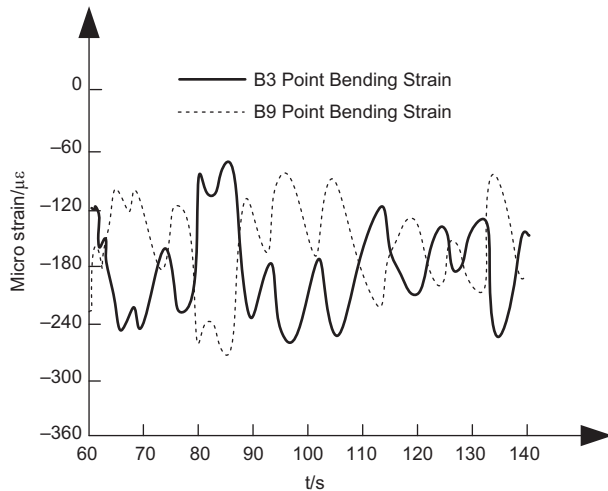
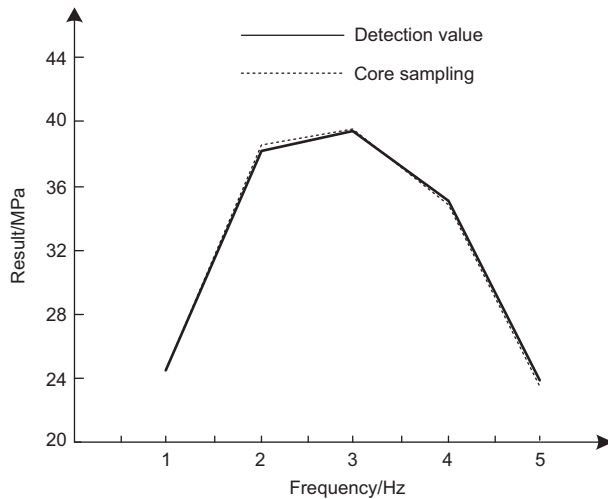


Fig. 9. Bending strain comparison of vibration devices at corresponding positions on two walls of diversion tunnel.

TABLE III. TEST RESULTS OF CONCRETE LINING THICKNESS.

Design value/m	Test value/m					Mean value
	First test	Second test	Third test	Fourth test	Fifth test	
0.5	0.51	0.48	0.53	0.49	0.53	0.51

**Fig. 10.** Comparison of concrete strength test results with drilling core sampling results.

When the design value of concrete lining thickness is 0.5 m, the actual construction value detected by the proposed method is about 0.5 m, which proves that the accuracy of the proposed method is better. The pore structure and interfacial bonding of the concrete are improved by adding appropriate amount of silica fume into the shotcrete. After spraying, the specimen is cured in the humid environment of the tunnel for 1 day and then demolded to obtain the core sample. The sample size is 450 mm × 450 mm × 120 mm. In **figure 10**, the concrete strength test results are compared with the core drilling sampling results. The results show that the compressive strength of the sample increases first and then decreases with the increase of the loading frequency. At the same time, the error interval between the core sampling results and the test values of the research method is 0.1-0.4MPa. The compressive strength of concrete obtained by core drilling is very consistent with the results obtained by the proposed method. that the error interval between the core sampling results and the test values of the proposed method is 0.1-0.4 MPa. The compressive strength of concrete obtained by core drilling is in good agreement with the results obtained by the proposed method.

DISCUSSION

With the large-scale development of water resources and hydropower resources in China and the state's poverty alleviation and development in remote mountainous areas, there are fewer and fewer hydropower stations with good physical and geographical conditions, and more and more small-scale diversion hydropower stations can be developed in remote mountainous areas. In the construction of hydropower projects, the concrete lining technology of headrace tunnel is gradually mature, but for the lining construction of saturated sand layer, most of them use manual dumping, the construction method is single, and the production efficiency is low. Therefore, the construction method and concrete lining equipment are more and more important in shortening the straight-line construction period. Practical operation of diversion tunnel in power station proves that short-distance pouring of materials on working face with small concrete pump can save labor, improve production efficiency, decrease waste and construction speed is fast, and it is a good method of economic, efficient and quality assurance.

The additional bending strain at each measuring point of the tunnel wall can be regarded as the superposition of the additional strain caused by the gentle increase of soil and water pressure and the additional vibration strain in the process of vibration, the former being the main part. The additional internal force on the tunnel wall section caused by earthquake is smaller than that under the original static force, but the total value increases obviously, which should be fully considered in the structural design. Because the additional internal force of the structure is mainly affected by the change of soil-water pressure during liquefaction of foundation, the practical design method of structure seismic response under liquefaction of saturated sand foundation can be considered according to the change law of soil-water pressure in liquefied foundation.

CONCLUSIONS

In this study, two ways are used to test the effect of tunnel concrete lining. The reflection characteristics

of impact elastic wave, the relationship between wave and concrete strength, and the attenuation characteristics of surface wave are used to better solve the problem of testing the thickness and strength of concrete lining of diversion tunnel. The two detection methods provide double guarantee for the effect of high-quality tunnel lining. The practicability and testing accuracy of this method are preliminarily verified by engineering trial and comparison of boreholes and sampling. It is worth further trial, which will create conditions for the popularization and application of underground water diversion tunnel lining in saturated sand stratum in the future.

ACKNOWLEDGMENT

The Research is Supported by 2020 Open Fund Research Project of Meteorological Disaster Prediction, Early Warning and Emergency Management Research Center in CUIT (Grant Number ZHYJ20-YB08).

REFERENCES

- Aboukila E.F. and Norton J.B. (2017). Estimation of saturated soil paste salinity from soil-water extracts. *Soil Science* 182(3), 107-113. <https://doi.org/10.1097/SS.000000000000197>
- Ahmed A.A., Saaid I.M. and Akhir N.A.M. (2017). Graft copolymerization of n-isopropylacrylamide and acrylic acid on bentonite colloids for in-depth fluid diversion. *Energy & Fuels* 31(4), 3537-3545. <https://doi.org/10.1021/acs.energyfuels.6b02507>
- Brown T.S., Du S., Eruslu H. and Sayas F.J. (2018). Analysis of models for viscoelastic wave propagation. *Applied Mathematics & Nonlinear Sciences* 3(1), 55-96. <https://doi.org/10.21042/AMNS.2018.1.00006>
- Chen F.X., Jin Z.Q., Wang E.D. and Wang L.Q. (2021). Relationship model between surface strain of concrete and expansion force of reinforcement rust. *Scientific Reports* 11(1), 4208. <https://doi.org/10.1038/s41598-021-83376-w>
- Chen F.X., Zhong Y.C., Gao X.Y., Jin Z.Q., Wang E.D., Zhu F.P., Shao X.X. and He X.Y. (2020). Non-uniform model of relationship between surface strain and rust expansion force of reinforced concrete. *Scientific Reports* 11(1), 8741. <https://doi.org/10.1038/s41598-021-88146-2>
- Fernández-Pousa C.R. (2018). Perfect phase-coded pulse trains generated by Talbot effect. *Applied Mathematics & Nonlinear Sciences* 3(1), 23-32. <https://doi.org/10.21042/AMNS.2018.1.00003>
- Galkaduwa M.B., Hettiarachchi G.M., Kluitenberg G.J. and Hutchinson S.L. (2017). Transport and transformation of selenium and other constituents of flue-gas desulfurization wastewater in water-saturated soil materials. *Journal of Environmental Quality* 46(2), 384. <https://doi.org/10.2134/jeq2016.09.0335>
- Gao W., Zhu L., Guo Y. and Wang K.Y. (2017). Ontology learning algorithm for similarity measuring and ontology mapping using linear programming. *Journal of Intelligent & Fuzzy Systems* 33(5), 3153-3163. <https://doi.org/10.3233/JIFS-169367>
- He L., Shen J. and Zhang Y. (2018). Ecological vulnerability assessment for ecological conservation and environmental management. *Journal of Environmental Management* 206(15), 1115-1125. <https://doi.org/10.1016/j.jenvman.2017.11.059>
- Hu A., Fu P. and Xia C. (2018). Horizontal impedances of saturated soil layer with radially inhomogeneous boundary zone. *Soil Dynamics and Earthquake Engineering* 111(4), 184-192. <https://doi.org/10.1016/j.soildyn.2018.04.012>
- Huo W.B., Li Z.J., Wang J.F. and Cheng Y. (2018). Multiple hydrological models comparison and an improved Bayesian model averaging approach for ensemble prediction over semi-humid regions. *Stochastic Environmental Research and Risk Assessment* 33(6), 217-238. <https://doi.org/10.1007/s00477-018-1600-7>
- Khellat F. and Khormizi M.B. (2018). A global solution for a reaction-diffusion equation on bounded domains. *Applied Mathematics & Nonlinear Sciences* 3(1), 15-22. <https://doi.org/10.21042/AMNS.2018.1.00002>
- Klaver P., Rutyna J. and Collins D. (2017). Investigation and mitigation of street flooding events at a combined sewer overflow storage tunnel diversion structure: Portland case study. *Proceedings of the Water Environment Federation* 2017(15), 572-590. <https://doi.org/10.2175/193864717822153274>
- Lakshminarayana G., Vajravelu K., Sucharitha G. and Sreenadh S. (2018). Peristaltic slip flow of a Bingham fluid in an inclined porous conduit with joule heating. *Applied Mathematics & Nonlinear Sciences* 3(1), 41-54. <https://doi.org/10.21042/AMNS.2018.1.00005>
- Lan M.Y.J., Zheng M.B.M., Shi T., Ma C.C., Liu Y.M. and Zhao Z.F. (2022). Crack resistance property of carbon nanotubes-modified concrete. *Magazine of Concrete Research* 74(22), 1-33. <https://doi.org/10.1680/jmacr.21.00227>
- Li H.L., Li Y. and Yao Z.F. (2019). Simulation of thermal field of power cable installed in traffic tunnel. *Computer Simulation* 36(02), 59-62. <https://doi.org/10.3969/j.issn.1006-9348.2019.02.014>
- Lu J.F., Ding J.J., Fan Z. and Liu M.H. (2017). Response of a circular tunnel embedded in saturated soil to a

- series of equidistant moving loads. *Acta Mechanica* 228(10), 3675-3693. <https://doi.org/10.1007/s00707-017-1893-5>
- Manitaras T.I. and Papadarakakis M. (2017). Footing settlement on a consolidating soil layer with stochastic properties. *Transport in Porous Media* 117(3), 507-524. <https://doi.org/10.1007/s11242-017-0844-x>
- Peng P., Cheng H.X. and Chen X.C. (2017). Estimation of state of charge of Li-ion battery based on adaptive Kalman filtering. *Chinese Journal of Power Sources* 41(11), 1541-1544. <https://doi.org/10.3969/j.issn.1002-087X.2017.11.010>
- Tian P., Lu H., Feng W. and Guan Y.L. (2020). Large decrease in streamflow and sediment load of Qinghai - Tibetan Plateau driven by future climate change: A case study in Lhasa River Basin. *Catena (Giessen)* 187(2-4), 104340. <https://doi.org/10.1016/j.catena.2019.104340>
- Walker X.J., Baltzer J.L., Cumming S.G., Day N.J., Johnstone J.F., Rogers B.M., Solvik K., Turetsky M.R. and Mack M.C. (2018). Soil organic layer combustion in boreal black spruce and jack pine stands of the Northwest Territories, Canada. *International Journal of Wildland Fire* 27(2), 125-134. <https://doi.org/10.1071/WF17095>
- Walsh R., Nasir O. and Calder N. (2018). Combining TOUGH2 and FLAC3D to solve problems in underground gas storage. *Transport in Porous Media* 123(12), 501-519. <https://doi.org/10.1007/s11242-017-0976-z>
- Wang X., Zhu Z. and Liu Z. (2017). Euler - lagrange two - phase flow large eddy simulation of construction ventilation in diversion tunnel. *Journal of Tianjin University* 50(1), 725-731.
- Wu G., Chen W. and Tian H. (2017). Numerical evaluation of a yielding tunnel lining support system used in limiting large deformation in squeezing rock. *Environmental Earth Sciences* 77(12), 439. <https://doi.org/10.1007/s12665-018-7614-0>
- Wu J.Z., Yuan J.B. and Siddiqui M.K. (2018). Independent set conditions for all fractional (g, f, n', m)-critical deleted NFV networks. *Journal of Intelligent & Fuzzy Systems: Applications in Engineering and Technology* 35(4), 4495-4502. <https://doi.org/10.3233/JIFS-169768>
- Xu D.P., Feng X.T. and Chen D.F. (2017). Constitutive representation and damage degree index for the layered rock mass excavation response in underground openings. *Tunneling & Underground Space Technology Incorporating Trenchless Technology Research* 64(4), 133-145. <https://doi.org/10.1016/j.tust.2017.01.016>
- Xue X.N., Gao S.P., Peng H.M. and Wu H.H. (2019). Density peaks clustering algorithm based on K-nearest neighbors and classes-merging. *Journal of Jilin University (Science Edition)* 57(1), 111-120. <https://doi.org/10.13413/j.cnki.jdxblxb.2017479>
- Yang C., Gao F. and Dong M. (2020). Energy efficiency modeling of integrated energy system in coastal areas. *Journal of Coastal Research* 103(sp1), 995. <https://doi.org/10.2112/SI103-207.1>
- Yang J.B., Zhang J.Y. and Song P.Y. (2017). Multi-objective optimization of energy management strategy for a tramway with onboard energy storage system. *Journal of Power Supply* 15(05), 137-143. <https://doi.org/10.13234/j.issn.2095-2805.2017.5.137>
- Yu D., Mao Y., Gu B., Nojavan S., Jermisittiparsert K. and Nasser M. (2020). A new LQG optimal control strategy applied on a hybrid wind turbine/solid oxide fuel cell/ in the presence of the interval uncertainties. *Sustainable Energy, Grids and Networks* 21(03), 100296. <https://doi.org/10.1016/j.segan.2019.100296>
- Yu F.H. (2019). Design and analysis of intelligent three dimensional parking lot control system based on PLC technology. *Automation & Instrumentation* 231(01), 86-88+92. <https://doi.org/10.14016/j.cnki.1001-9227.2019.01.080>
- Zhao C. and Li J. (2020). Equilibrium selection under the Bayes-based strategy updating rules. *Symmetry* 12(5), 739. <https://doi.org/10.3390/sym12050739>
- Zhu D.J., Pi X.S. and Yue X.C. (2017). A method on direct arrival wave suppression for high frequency hybrid sky-surface wave radar. *Journal of China Academy of Electronics and Information Technology* 12(01), 31-36. <https://doi.org/10.3969/j.issn.1673-5692.2017.01.006>
- Ziaei A. and Ahangari K. (2018). The effect of topography on stability of shallow tunnels case study: The diversion and conveyance tunnels of Safa Dam. *Transportation Geotechnics* 14(12) 126-135. <https://doi.org/10.1016/j.trgeo.2017.12.001>
- Zou D., Teng X., Kai C. and Yu X. (2018). An extended polygon scaled boundary finite element method for the nonlinear dynamic analysis of saturated soil. *Engineering Analysis with Boundary Elements* 91(02), 150-161. <https://doi.org/10.1016/j.enganabound.2018.03.019>
- Zuo, X., Dong, M.Y., Gao, F.K. and Tian S.M. (2020). The modeling of the electric heating and cooling system of the integrated energy system in the coastal area. *Journal of Coastal Research* 103(sp1), 1022. <https://doi.org/10.2112/SI103-213.1>